Journal of Zhejiang University-SCIENCE A (Applied Physics & Engineering)
ISSN 1673-565X (Print); ISSN 1862-1775 (Online)
www.zju.edu.cn/jzus; www.springerlink.com
E-mail: jzus@zju.edu.cn

Fatigue and fracture behavior of nickel-based superalloy Inconel 718 up to the very high cycle regime*

Xian-feng MA[†1], Zheng DUAN[1], Hui-ji SHI[†‡1], Ryosuke MURAI[2], Eiichi YANAGISAWA[2]

([1]*Applied Mechanics Laboratory, Department of Engineering Mechanics, School of Aerospace, Tsinghua University, Beijing 100084, China*)

([2]*Mitsubishi Heavy Industries, Ltd., Tokyo, Japan*)

[†]E-mail: maxianfeng@gmail.com; shihj@mail.tsinghua.edu.cn

Received Apr. 15, 2010; Revision accepted Aug. 12, 2010; Crosschecked Sept. 18 , 2010

Abstract: The fatigue and fracture behavior of nickel-based superalloy Inconel 718 was investigated up to the very high cycle regime under rotary bending tests at room temperature. It was found that this superalloy can still fracture after exceeding 10^7 cycles. Fractographic analysis revealed that there was a transition from fatigue crack initiation at multi-sites to single initiation with decreasing stress levels. The fracture surface can be divided into four areas according to the appearance, associated with fracture mechanics analysis of the corresponding stress intensity factors. The fracture mechanism dominant in each area was disclosed by scanning electron microscope examination and analyzed in comparison with those obtained from the crack growth tests. Subsequently, life prediction modeling was proposed by estimating the crack initiation and propagation stage respectively. It was found that Chan (2003)'s model for initiation life and the Paris law for growth life can provide comparable predictions against the experimental life.

Key words: Nickel-based superalloy, High cycle fatigue (HCF), Fatigue crack initiation, Crack growth, Life prediction
doi:10.1631/jzus.A1000171 **Document code:** A **CLC number:** TB3; V25

1 Introduction

Nickel-based superalloys are widely used for key components of jet engines and gas turbines for their high yield strength, excellent fatigue resistance, and good corrosion endurance in severe conditions (Chen *et al.*, 2000; 2005). Much attention has been paid to their fatigue behaviour due to the problem of fatigue failures in aircraft systems induced by the alternating stress in service (Chen *et al.*, 2000; Kobayashi *et al.*, 2005). For the satisfactory cost/performance ratio and excellent process capability, Inconel 718 (IN718) superalloy has been predominantly used in aeronautic engine components, such as turbine disc and shaft, compressor disc, compressor blade, and so on (Chen *et al.*, 2005). During the past few decades, extensive investigations have been made on the low cycle fatigue (LCF) and high cycle fatigue (HCF) properties of IN718, such as the effect of temperature on the cyclic stress-strain response and LCF life associated with the deformation microstructures (Fournier and Pineau, 1977; Reger and Remy, 1988a; 1988b), the factors (temperature, environment, and loading parameters, etc.) influencing fatigue crack growth (Bache *et al.*, 1999; Remy *et al.*, 2007; Leo Prakash *et al.*, 2009), the creep-fatigue-oxidation interactions (Pineau, 1989; Leo Prakash *et al.*, 2009), the mechanism-based modeling of fatigue life prediction (Alexandre *et al.*, 2004), and so on.

Nowadays, the very high cycle fatigue (VHCF) properties of high strength metals have become more and more significant, ever since the finding of fatigue failure beyond 10^7 cycles in high-strength steels (Masuda and Tanaka, 1986). The subsequent studies on many ferroalloys (Murakami *et al.*, 1991; Sakai *et*

‡ Corresponding author

* Project supported by the National Natural Science Foundation of China (Nos. 10872105 and 51071094), and the Mitsubishi Heavy Industries, Ltd., Japan

al., 2006) prove that the conventional fatigue limit in HCF disappears in the VHCF regime and there is a transition of fatigue crack initiation from the surface to the internal defects at around 10^6–10^7 cycles (Sakai *et al.*, 2002). Furthermore, it is recognized that the gigacycle fatigue failure of high strength steels is preferentially initiated from interior inclusions, giving the appearance of a fish-eye (Murakami *et al.*, 1991; Sakai *et al.*, 2006). Recent studies on duplex steels, e.g., the austenite/martensite and ferrite/martensite duplex steels (Chai, 2006), reveal the subsurface non-defect crack initiation after VHCF fracture, indicating another type of initiation mode. Compared to the comprehensive investigation and understanding of the VHCF properties of steels (Sakai *et al.*, 2002; Wang *et al.*, 2002) and Al-alloys (Wang *et al.*, 2006), few studies exist on nickel-based superalloys, e.g., IN718 superalloy (Yan *et al.*, 2003). Yan *et al.* (2003) performed a rotary bending fatigue test on IN718 and found that it did not show gigacycle fatigue failure at room temperature, but did at 500 °C. However, another study (Chen *et al.*, 2005), under ultrasonic frequency, revealed that fatigue fracture of IN718 occurred between 10^7 and 10^8 cycles. Insofar as the experimental work suggests, it is still argumentative whether this superalloy under practical loading would show VHCF or not. Furthermore, it is known that the fatigue crack initiation process becomes increasingly important with the extension of fatigue life. A deeper insight into VHCF damage is expected to be achieved from this study under conventional frequency, which would pave the way for the safety evaluation after long-term service and the long-life design of critical turbine components.

In this study, the HCF and VHCF properties of IN718 superalloy were investigated under rotating bending fatigue test at room temperature. With the help of scanning electron microscope (SEM), fractographic analyses were performed to disclose the fracture features of specimens in different life ranges. The predominant fracture mechanism in each region of fatigue crack initiation/propagation was discussed in association with the fracture mechanics calculation. Finally, based on the understanding of crack initiation and propagation stages, the fatigue life was approximately predicted by the sum of the life cycles for the initiation and propagation of fatigue cracks.

2 Material and experimental procedure

The material under investigation was a nickel-based superalloy IN718 (GH4169 in China, and Nc19FeNb in France) with a chemical composition (%, w/w) of 0.02C, 0.12Mn, 0.11Si, 0.009P, 0.001S, 18.67Cr, 3.09Mo, 0.09Co, 0.01Cu, 0.66Al, 0.90Ti, 18.67Fe, 0.004B, 5.12Nb and Ta, and balanced Ni. The heat treatment of the alloy was as follows: solution at 970 °C for 1 h, water quenched, directly aged at 720 °C for 8 h, then furnace cooled to 620 °C at a rate of 50 °C/h and aged at 620 °C for another 8 h followed by air-cooling. The basic mechanical properties of this superalloy at room temperature were obtained by tensile test (Table 1). A typical micrograph of the IN718 superalloy is shown in Fig. 1. The microstructure consists of grey blocks of carbides and fine lenticular particles of δ phases (Ni_3Nb) distributed in the matrix. The nearly equiaxed grains of Ni-rich face-centered cubic (FCC) solid solution (γ phase) can be seen, exhibiting average grain size of around 10 μm.

Table 1 Mechanical properties of the IN718 superalloy employed in this study (at room temperature)

0.2% yield stress (MPa)	Tensile strength (MPa)	Elongation (%)	Reduction of area (%)	Vickers hardness
1220	1390	23.0	39.5	426

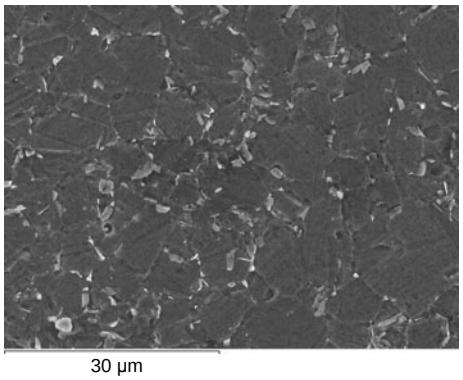

Fig. 1 SEM micrograph showing the typical microstructure of IN718

The specimen is in the shape of an hourglass, as shown in Fig. 2. The stress concentration factor is calculated by finite element analysis with ABAQUS to be α=1.024. Prior to fatigue testing, all the specimens were polished to remove the scratches along the

circumferential direction. Fatigue tests were performed in ambient atmosphere at room temperature using a four-axis cantilever-type rotating bending test machine, which was operated at a frequency of 52.5 Hz (i.e., 3150 r/min). This multi-type fatigue testing machine was developed by the Research Group for Statistical Aspects of Material Strength in Japan (Sakai *et al.*, 2002), which can be used to test four fatigue specimens simultaneously. No evident increase of temperature is found during the test due to the relatively low frequency, as proposed by Sakai *et al.* (2006). Hence, the effect of heat or oxidation can be excluded in this study. A weight is appended from the outer end of each specimen by a bearing and a spring to generate stress ratio of $R=-1$.

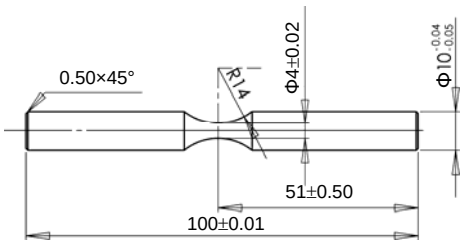

Fig. 2 Specimen for fatigue testing (unit: mm)

3 Results

3.1 *S-N* curve

Fig. 3 shows the *S-N* curve of IN718 obtained from the cantilever-type rotary bending fatigue tests at room temperature under the load ratio of $R=-1$. The fatigue life increases with decreasing stress amplitude and the *S-N* curve appears to continuously decline as the life extends. Note that fatigue failure of this superalloy continues to occur after exceeding 10^7 cycles. The longest fatigue life of the fractured specimens is 2.04×10^8 cycles, which takes more than 40 d of fatigue testing. The test result can be regarded as the direct evidence of IN718 fracture in the VHCF regime at room temperature.

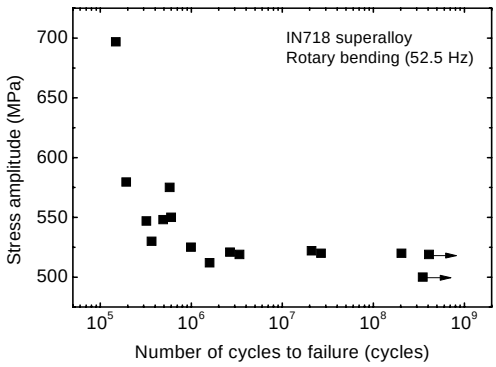

Fig. 3 Fatigue test S-N curve of IN718 at room temperature under $R=-1$

3.2 Fractography

Each fatigued specimen was subjected to SEM observations to examine the fracture features. Fig. 4 shows the overall appearance of the fracture surfaces at different stress levels, with the initiation site marked by arrow. At high stress levels, fatigue cracks initiated from multiple initiation sites, as shown in Figs. 4a–4c. In these cases, as the propagation of these multiple cracks are not necessarily on the same plane, the final coalescence of multiple cracks will lead to macroscopic fluctuant fracture surfaces. With decreasing stress, the number of crack initiation sites reduces correspondingly. Fracture due to a single fatigue crack (visible on the fracture surface) becomes predominant for specimens with longer fatigue lives ($>10^6$ cycles, e.g., Fig. 4d). In this case, the fracture surface generated by the single main crack generally has much less roughness. Furthermore, it is indicated that the fatigue crack preferentially takes place at the specimen surface in the conditions in Fig. 4.

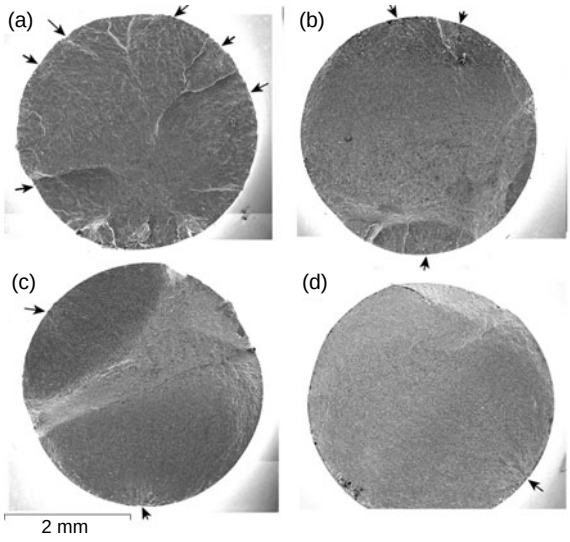

Fig. 4 Overview of the typical fracture surfaces in HCF regime. (a) σ_a=697 MPa, $N_f=1.481\times10^5$ cycles; (b) σ_a=548 MPa, $N_f=4.91\times10^5$ cycles; (c) σ_a=525 MPa, $N_f=9.912\times10^5$ cycles; (d) σ_a=519 MPa, $N_f=3.3894\times10^6$ cycles

In addition, from the above fractographies, it is found that the fracture surfaces of most specimens can be generally divided by appearance into four typical areas: (I) a relatively flat surface area at the initial stage (indicated by dashed lines in Fig. 5); (II) a distinctly rough area outside the initial flat area with propagation traces (Fig. 5); (III) a wide fracture surface with radial streaks along the crack propagation direction; and, (IV) dimples due to overload. The four areas reflect the different stages during crack initiation and propagation (Sakai *et al.*, 2002). The corresponding feature of each area will be further analyzed below.

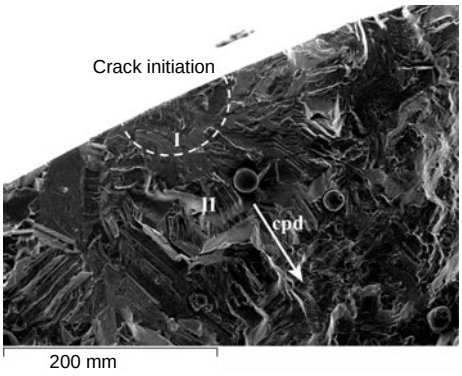

Fig. 5 Fracture surface of a specimen fatigue tested at σ_a=547 MPa, N_f=3.212×10^5 cycles (cpd: crack propagation direction)

When the stress amplitude is gradually decreased and approaching 520 MPa, the fatigue life shows sensitivity on the stress level (Fig. 3). A sample fractured beyond 10^7 cycles was examined by SEM to disclose the fracture behavior in the long-life regime. The four areas depicted above are marked in Fig. 6a. Fig. 6b is a magnification of the area marked by "I", which shows the crack initiated from surface grains. And the crystallographic fracture is similar as those observed in HCF regime in Fig. 5. The facet is about 45° inclined to the specimen axis, indicating that the fatigue crack grows along the planar slip on {111} plane which is favorable in FCC superalloys (Kobayashi *et al.*, 2005; Ma *et al.*, 2008). This is in accordance with the in-situ SEM examination of IN718 (Andersson and Persson, 2004) which proved the dominance of transgranular crack growth mechanism at room temperature under various SIF ranges ΔK and maximum stress values.

A cleavage-like fracture is visible after the cracks extend over several grains in depth and becomes predominant with the advance of crack length (Area II). The quasi-cleavage cracking feature is clear in Fig. 6c, which is about 300 μm from the nucleation site. In the early stage of Area III, fine striations appear together with the quasi-cleavage fracture. With the increase in stress intensity, the fatigue striations become obvious (Fig. 6d), indicating the stable crack propagation in Paris regime when the pure fatigue crack growth is dominated by the usual plastic blunting mechanism (Mercer *et al.*, 1999). In the high ΔK regime of Area III, which is close to the center of the sample section, the ductile-dimple fracture mode can be observed in Fig. 6e, in addition to fracture of particles ahead of the crack tip. Fig. 6f shows the classical ductile-dimpled fracture mechanism in the tensile overload region (Area IV), which is similar to the 'static' fracture mode in the high ΔK fatigue regime in Fig. 6e. The presence of secondary cracks may be evidence of the extensive plastic deformation ahead of the crack tip.

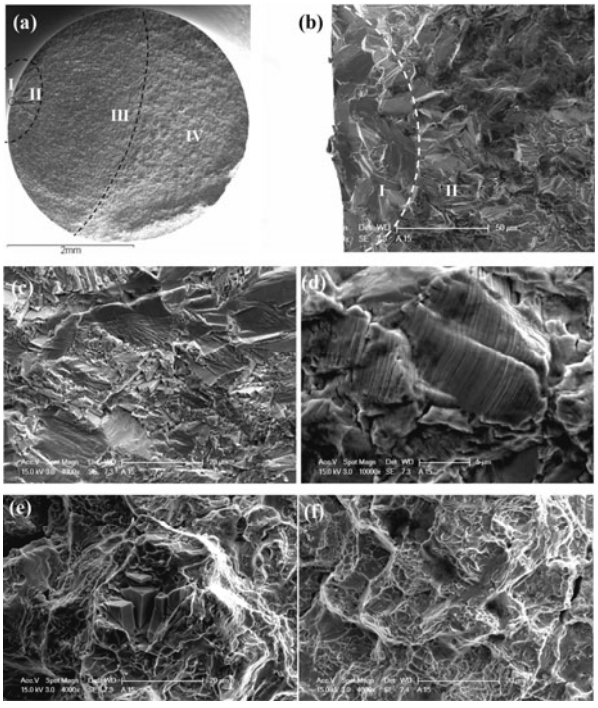

Fig. 6 Fracture surface of a specimen tested at σ_a=520 MPa, N_f=2.66265×10^7 cycles. (a) Overview of fracture surface; (b) Crack nucleation site and the initial crack propagation; (c) Quasi-cleavage fracture at a distance of 300 μm from the nucleation site; (d) Striations corresponding to stable crack propagation (about 1 mm from nucleation site); (e) High ΔK regime of rapid crack growth (about 1.7 mm from nucleation site); (f) Tensile overload region of the specimen

Two other specimens with fatigue lives longer than 10^7 cycles were examined carefully under SEM. Fig. 7 shows the crack nucleation site (Area I) and crack propagation in the early stage (Area II), revealing single fatigue crack for both specimens. Furthermore, it is noted that the fatigue fracture initiation site is shifted inwards (Sakai *et al.*, 2002; 2006; Wang *et al.*, 2002; Yan *et al.*, 2003), tending to originate from the subsurface grain, as indicated by dashed lines in Figs. 7a and 7b. As there are no evident inclusions in this superalloy like those widely found in high-strength steels (e.g., SUJ2), fish-eye was absent in the VHCF fracture of IN718 insofar as we observed. For the specimen with the longest life of 2.04×10^8 cycles in Fig. 7b, large radial ridges can be observed in the propagation direction in Area II after the crack nucleated from the subsurface. It can be further seen in Fig. 7b that there are many tyre patterns formed beyond the initiation zone, which is somewhat unusual and rarely reported in IN718 superalloy. However, other researchers (Chu *et al.*, 2008) also observed tyre patterns with a uniform interval of about 10 μm along the propagation direction in the directionally solidified superalloy DZ951. Explanation for this behavior is unavailable in literature to date, and it appears similar to the ridges formed during fatigue crack propagation, but with a smaller scale (Chan and Leverant, 1987; Mercer *et al.*, 1999). Additional investigation is underway to examine the dislocation substructure, which may help to understand the fracture behavior and disclose possible effects of the precipitates. The classical striation type of fracture in Area III, and the ductile dimples due to overload in Area IV are quite similar to the specimen (σ_a=520 MPa, N_f =2.66265×10^7 cycles) in Fig. 6.

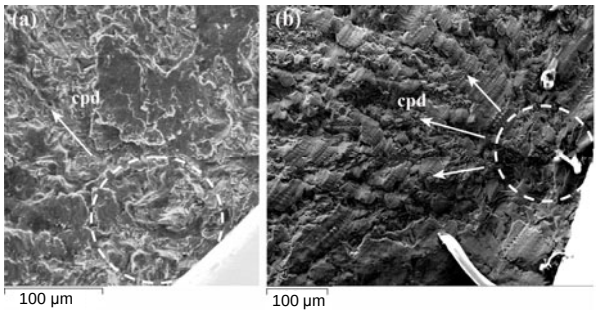

Fig. 7 Crack nucleation site and the initial crack propagation of fatigued specimen. (a) σ_a=522 MPa, N_f=2.099×10^7 cycles; (b) σ_a=520 MPa, N_f=2.04×10^8 cycles (cpd: crack propagation direction)

4 Discussion

4.1 Fatigue crack initiation

The above fractographic observations revealed that the fatigue crack initiation sites were different depending on the stress amplitude and fatigue life. This dependence is demonstrated in Fig. 8. It is found that the fatigue crack initiation exhibits a transition from multiple origins to single origin with increasing fatigue life. Fatigue fracture in the high cycle range is caused by the gradual growth of microcracks initiated in slip bands on the specimen surface, because the surface has favorable conditions for the nucleation and growth of cracks compared to the interior region due to geometric-mechanical conditions (Forsyth, 1957; Suresh, 1998). It is featured in the rotary bending fatigue test that the normal stress on the cross section has a radial gradient, which makes the crack preferentially initiate from the outer surface. In comparison with uniaxial tensile fatigue, it is believed to be more difficult for fatigue damage accumulation to occur at internal defect under rotary bending loading due to lower interior stress.

Moreover, under high stress levels, crystallographic slip systems can be activated in more than one surface grains at different locations, leading to initiation at multi-sites (Suresh, 1998; Chu *et al.*, 2008). This is similar to the multiple cracks in other materials due to stress concentrators, such as oxide layer (Fournier *et al.*, 2008), casting micropores (Ma *et al.*, 2008), and pickling pits (Chaussumier *et al.*, 2010). On the other hand, with a low stress level, only the most easily-operated slip can be induced by the localized plastic deformation during crack nucleation. Noted that specimens with a single initiation site

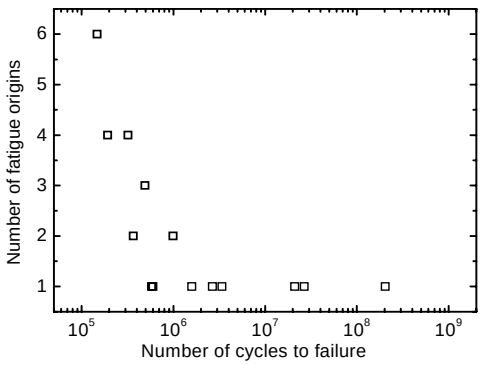

Fig. 8 Number of crack initiation sites versus fatigue life cycles

generally show longer fatigue life than those with multiple fatigue origins under comparable stress.

4.2 Fatigue crack propagation

To clarify the fatigue fracture mechanisms in different stages of HCF or VHCF, the dimensions of the marked regions on each fracture surface (as shown in Fig. 6) are measured. It is expected that the crack will propagate after the formation of the relative flat area (Area I) in the vicinity of the crack origin, i.e., the surface semi-elliptical (Fig. 5 and Fig. 6b) or subsurface elliptical or circular zone (Figs. 7a and 7b). Area I is generally on the order of several grain diameters, which is identified to be the initiation region subsequently in this section. The nominal stress intensity factor (SIF) at the initiation site can be calculated (Anderson, 1991; Murakami *et al.*, 1991):
for surface crack initiation,

$$K = \sigma\sqrt{\pi b}\, F_{\mathrm{I}}/E(k), \tag{1}$$

for subsurface crack initiation,

$$K = 0.5\sigma\sqrt{\pi\sqrt{\mathrm{area}_{\mathrm{ini}}}}, \tag{2}$$

where σ is the applied nominal stress level (MPa), b is the semi-minor axis of the ellipse (m), F_{I} is the shape factor (Anderson, 1991), $E(k)$ is the second ellipse integral (Anderson, 1991), and $\sqrt{\mathrm{area}_{\mathrm{ini}}}$ is the size of subsurface crack initiation site (m).

Values of the SIF ranges at the initiation sites (ΔK_{ini}) are summarized in Fig. 9, which appear to be within a range of 9–15 MPa·m$^{1/2}$ at room temperature. Moreover, the test results of crack growth obtained by other researchers are plotted in Fig. 10 for comparison. The fatigue crack growth (FCG) test by Mercer *et al.* (1999) was carried out by single edge notched bending (SENB) specimens and another research was on compact tension (CT) specimens (He *et al.*, 2006), whereas Chen *et al.* (2000)'s was performed by rotary bending. It was found that the SIF values calculated above are roughly comparable with the crack propagation threshold ΔK_{th} for this superalloy (Fig. 10). This agrees with the above assumption that the initial facet area roughly corresponds to the crack initiation zone, beyond which the fatigue life is dominated by crack growth. However, as the tests in Fig. 10 are mainly in long crack regime without the stage of small crack propagation, Fig. 10 is employed here for comparative discussion. Furthermore, ΔK_{ini} decreases slightly with increasing fatigue life, which is similar to the results in SUJ2 (Shiozawa *et al.*, 2001). It is rationalized that a crack nucleated internally at a lower stress amplitude can propagate under a smaller SIF.

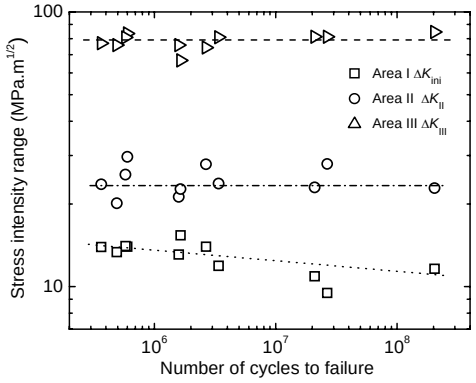

Fig. 9 Fatigue life versus ΔK_{ini}, ΔK_{II}, or ΔK_{III}

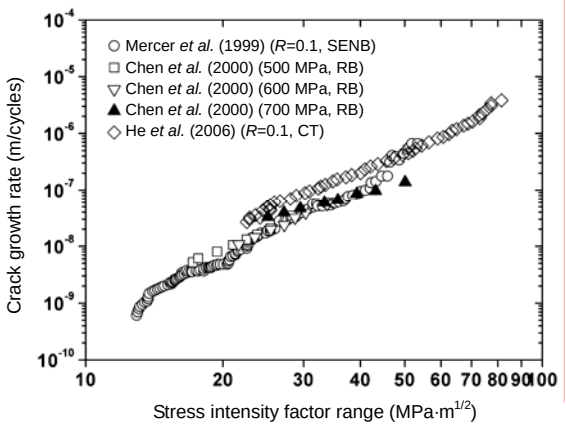

Fig. 10 Crack growth rate as a function of ΔK for IN718 at room temperature in different tests
SENB: single edge notched bending; CT: compact tension; RB: rotary bending; *R*: stress ratio

The SIF values at the outer boundaries of Areas II and III, i.e., ΔK_{II} and ΔK_{III} are calculated by Eq. (1) and plotted in Fig. 9 in terms of the fatigue life. ΔK_{II} is distributed in the range of 19–29 MPa·m$^{1/2}$, which implies that Area II roughly corresponds to the stage between near-threshold regime and lower Paris regime (Fig. 10). The SIF level is close to the test result of He *et al.* (2006) in Fig. 10, probably due to the same source (composition and heat treatment, etc.) of

IN718 superalloy material. In the near-threshold regime, the mechanism of fatigue crack propagation is by transgranular, crystallographic fracture in favored crystallographic slip systems induced by separation of atomic bonds directly ahead of the crack-tip, as reported in (Mercer *et al.*, 1999).

Striations can be observed in upper Paris regime as the crack propagates stably during RB loading cycles. The ΔK values when striations are dominated in Fig. 6 are approximately in the range of 37–55 MPa·m$^{1/2}$. This is coincident with Mercer *et al.* (1999)'s observation that the classical striations corresponding to greater levels of plasticity was observed at SIF ranges >35 MPa·m$^{1/2}$. In addition, results of ΔK_{III} in Fig. 9 fall within a band of 70–80 MPa·m$^{1/2}$ regardless of the fatigue life, which approximately accord with the fracture toughness K_{IC} or the fatigue fracture toughness of IN718 superalloy.

Consequently, the four areas defined by three dashed lines on the fracture surface correspond roughly to the crack initiation zone, near-threshold regime, Paris propagation regime followed by rapid propagation, and catastrophic fracture of tensile overload, respectively. The fatigue fracture mechanism dominated in each regime is comparable with the results of Mercer *et al.* (1999) and He *et al.* (2006) in fatigue crack growth tests.

4.3 Theoretical modeling of fatigue life

Previous researches (Antolovich and Jayaraman, 1983; Murakami *et al.*, 1991; Kobayashi *et al.*, 2005) have addressed the important roles of microstructure in fatigue crack initiation and propagation in metals. Recent fatigue-crack-initiation models try to incorporate microstructural parameters in a more direct and explicit manner (Tanaka and Mura, 1981; Venkataraman *et al.*, 1991; Chan, 2003; Alexandre *et al.*, 2004). Tanaka and Mura (1981) proposed dislocation models for treating fatigue crack initiation at slip-bands, inclusions and notches. Considering the dislocation-dipole mechanism along the slip band operating in a surface or subsurface grain, which finally leads to the fatigue crack initiation due to the stored energy in the dislocation dipoles, the number of cycles to crack initiation was given by

$$(\Delta\tau - 2\tau_f)^2 N_i = \frac{4\mu W_s}{\pi(1-\upsilon)d}, \tag{3}$$

where $\Delta\tau$ is the shear-stress range, τ_f is the friction stress of dislocation, μ is the shear modulus, d is the grain size, υ is Poisson's ratio, and W_s is the specific energy per unit area along the slip band.

The basic model of Tanaka and Mura (1981) in Eq. (3) has been modified by Venkataraman *et al.* (1991) to consider different initiation mechanisms. An extension of this model was made by Chan (2003) to include the crack size and some relevant microstructural parameters as

$$[\Delta\sigma - 2M\tau_f]^2 N_i = \frac{8cM^2\mu^2h^2}{0.005\pi(1-\upsilon)d^3}, \tag{4}$$

where M is the Taylor factor for the optimally oriented grain, taken to be 2 (Chan, 2003), h is the slip-band width, and c is the crack depth at crack initiation.

It can be seen that Eq. (4) describes the inverse relationship between fatigue initiation life and the grain size, which agrees with the experimental observed influence of grain size on fatigue performance (Venkataraman *et al.*, 1991; Chan, 2003; Kobayashi *et al.*, 2005). Moreover, it attempts to relate the fatigue initiation life to the fractographic feature of each specimen quantitatively through the crack initiation depth c. For IN718 herein, we take d as the grain size in the crack initiation zone. The term $M\tau_f$ represents the fatigue limit stress, as suggested by Chan (2003). Regarding the continuous descending *S-N* curve in this study, it is taken as the fatigue strength at 4×10^8 cycles for instance, i.e., approximately 519 MPa, which is a more conservative choice than the fatigue limit at 10^7 cycles. h is specified as 0.015 μm, which is close to the slip-band width of IN100 superalloy (Chan, 2003).

On the other hand, the fatigue crack propagation life can be calculated, assuming that the crack growth rates evaluated from Fig. 10 are valid as soon as the crack is long enough for stage II propagation. A similar assumption is also used in the research of martensitic steel (Fournier *et al.*, 2008). The number of cycles needed for the crack to grow from the initial size a_0 to the final crack length a_f, i.e., the crack growth life N_p, is given by

$$N_p = \frac{a_0^{(1-n/2)} - a_f^{(1-n/2)}}{C\Delta\sigma^n\beta_1^n\pi^{n/2}(n/2-1)}, \tag{5}$$

where the geometry constant $\beta_1 = 0.5\sqrt{\pi}$ (Anderson, 1991), a_0 is taken as the crack initiation depth c in the following calculation. a_f is set equal to the sample radius (2 mm), beyond which the sample is regarded as fractured. $\Delta\sigma$ is the applied stress range which assists the crack propagation. C and n follows the Paris law:

$$\frac{\mathrm{d}a}{\mathrm{d}N} = C(\Delta K)^n, \tag{6}$$

It is widely used that the total fatigue life can be estimated by the sum of fatigue crack initiation life and propagation life. Another study on IN718 (Alexandre *et al.*, 2004) with different grain sizes conducted life prediction based on the Tanaka and Mura (1981) model for Stage I initiation and Tomkins (1968) model for crack growth. In this study, the total fatigue life is obtained by summing up Eq. (4) and Eq. (5):

$$N_f = N_i + N_p = \frac{8cM^2\mu^2h^2}{0.005\pi(1-\upsilon)(\Delta\sigma - 2M\tau_f)^2 d^3} + \frac{c^{(1-n/2)} - a_f^{(1-n/2)}}{C\Delta\sigma^n\beta_1^n\pi^{n/2}(n/2-1)}. \tag{7}$$

For IN718 at room temperature, the Paris parameters can be obtained from the crack growth test data in Fig. 10. By curve fitting, the two parameters are given as

$$C = 3\times10^{-13},\ n = 4. \tag{8}$$

Finally, Eq. (8) is substituted into Eq. (7), together with other material parameters, to obtain the total fatigue life. Noted that for the specimens with crack initiation at multi-sites in this study, some assumptions should be made in the calculation of fatigue life. Strict treatment of multi-cracking and coalescence can be found in literature based either on complex numerical simulation (Chaussumier *et al.*, 2010) or on stochastic analysis introducing the crack density conservation law (Fedelich, 1998). Generally, assumptions on the distribution of crack size and location, crack evolution, coalescence condition, and so on should be used, which makes the life prediction quite complicated. Others roughly estimate the crack density and many simplifications are done to reflect the decrease of fatigue life by multi-cracks (Fournier *et al.*, 2008). Considering that it is beyond our understanding of the cracking of IN718 to rigorously handle the multiple cracks, an eclectic treatment is adopted here. That is, for those specimens with more than one initiation site, only the primary crack which occupies the largest portion of fracture surface is measured and used in the life calculation. It is based on the understanding that the primary crack controls the final rupture of the specimen. Furthermore, for multi-cracking specimens, the crack initiation length c would be smaller than that of single-crack specimen, reflecting the influence of multiple cracks and coalescence, whereas the original model of Tanaka and Mura (Eq. (3)) does not take into account this effect.

Replacing the expression of N_i in Eq. (7) by that of Eq. (3), the total fatigue life model based on Tanaka and Mura's can be obtained analogously. The fatigue lives predicted by both Tanaka and Mura's model and Chan's model are plotted with the experimental results in Fig. 11. Rational coincidence can be seen in most cases, i.e., the predicted results fall into the double-error band indicated by dashed lines. For the data point beyond the error band, the experimental fatigue life is unusually long; although it is subjected to a high applied stress. As a whole, Tanaka and Mura's model gives more conservative prediction than that of Chan's model, especially in the long life regime. It may be understood that Tanaka and Mura's model only considers the lifetime to initiate a crack with a size comparable to the grain diameter (Fournier *et al.*, 2008), whereas the crack initiation zone may cover several grains as observed in fractography, which partly explains why Tanaka and Mura's model underestimates the fatigue life. In general, calculating initiation life by Chan's model gives a relatively good life prediction of IN718 superalloy in the examined life regimes.

Noted that this model has the advantage of providing the proportion of the life consumed under each phase of crack initiation and crack propagation, and furthermore, the parameters involved are material constants or derived from ordinary test results. The model shows that the life cycles attributable to crack initiation become increasingly significant with decreasing stress amplitude. For those specimens

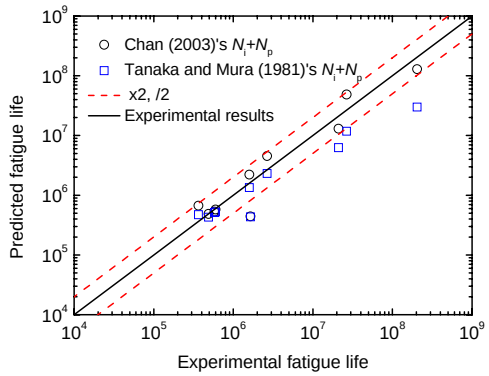

Fig. 11 Fatigue life prediction based on fatigue crack initiation and propagation

fatigued in high cycle regime, most of the fatigue life is consumed in Areas I and II, whereas Paris crack propagation in Area III takes relatively much less time, especially for long life fatigue. In the VHCF regime, the proportion of crack initiation life can be even more than 99% according to the model calculation, in agreement with Wang *et al*. (2002)'s results on high-strength steels. Test data of IN718 superalloy under completely reversed uniaxial fatigue (Socie, 1983) revealed that in LCF ($<10^5$ cycles), it took less than 40% of fatigue life to generate a crack of 100 μm, whereas this crack did not appear until about 90% of the total life cycles in HCF (10^6–10^7 cycles). It is thus increasingly accepted to predict the long fatigue life in terms of crack initiation and growth.

5 Conclusions

Nickel-based superalloy IN718 was subjected to RB fatigue tests up to the long life regime at room temperature. The conclusions obtained in this study are summarized as follows:

1. Fatigue failure of IN718 can still occur after 2.04×10^8 cycles at room temperature and the *S-N* curve appears in a continuously decreasing manner.

2. Fractographic analysis reveals a transition of fatigue crack initiation from multi-sites to single site when decreasing the stress amplitude, controlled by crystallographic slip in near-surface grains.

3. The fracture surface can be divided into four typical areas according to the appearance. Fracture mechanics analysis indicates that these four areas roughly correspond to (I) the crack initiation zone, (II) near-threshold regime, (III) Paris propagation regime followed by accelerated propagation regime, and (IV) the final catastrophic fracture due to overload, respectively.

4. The fatigue fracture mechanism dominated in each regime is comparable with those reported in FCG tests. Fatigue crack propagate in a transgranular, crystallographic fracture manner in the initiation and near-threshold regime. Quasi-cleavage fracture together with some fine striations is favorable in lower Paris fatigue regime. Relatively coarse striations are predominant in the upper Paris regime, governed by the classical crack-blunting mechanism. Accelerated crack growth in the high ΔK regime was attributed to ductile-dimpled fracture mode, accompanied with the fracture of distributed particles. In the tensile overload region, ductile dimples similar to static tensile overload and secondary cracks are common.

5. A total life prediction is performed based on the estimation of fatigue crack initiation and propagation, incorporating microstructural and fractographic parameters, which compares favorably with the experimental fatigue life.

Acknowledgements

The authors gratefully thank the Mitsubishi Heavy Industries, Ltd., Japan for financial supports, and Dr. Xie in the Institute of Mechanics, Chinese Academy of Sciences for help in setting up the fatigue tests.

References

Alexandre, F., Deyber, S., Pineau, A., 2004. Modelling the optimum grain size on the low cycle fatigue life of a Ni based superalloy in the presence of two possible crack initiation sites. *Scripta Materialia*, **50**(1):25-30. [doi:10.1016/j.scriptamat.2003.09.043]

Anderson, T.L., 1991. Fracture Mechanics: Fundamentals and Applications. CRC Press, Colorado, USA.

Andersson, H., Persson, C., 2004. In-situ SEM study of fatigue crack growth behaviour in IN718. *International Journal of Fatigue*, **26**(3):211-219. [doi:10.1016/S0142-1123(03)00172-5]

Antolovich, S.D., Jayaraman, N., 1983. The Effect of Microstructure on Fatigue Behavior of Nickel Base Alloys. Plenum Press, NY, USA.

Bache, M.R., Evans, W.J., Hardy, M.C., 1999. The effects of environment and loading waveform on fatigue crack growth in Inconel 718. *International Journal of Fatigue*,

21(Suppl. 1):69-77. [doi:10.1016/S0142-1123(99)00057-2]

Chai, G.C., 2006. The formation of subsurface non-defect fatigue crack origins. *International Journal of Fatigue*, **28**(11):1533-1539. [doi:10.1016/j.ijfatigue.2005.06.060]

Chan, K.S., 2003. A microstructure-based fatigue-crack-initiation model. *Metallurgical and Materials Transactions A*, **34**(1):43-58. [doi:10.1007/s11661-003- 0207-9]

Chan, K.S., Leverant, G.R., 1987. Elevated-temperature fatigue crack-growth behavior of Mar-M200 single-crystals. *Metallurgical and Materials Transactions A*, **18**(4):593-602. [doi:10.1007/BF02649475]

Chaussumier, M., Shahzad, M., Mabru, M., Chieragatti, R., Rezaï-Aria, F., 2010. A fatigue multi-site cracks model using coalescence, short and long crack growth laws, for anodized aluminum alloys. *Procedia Engineering*, **2**(1):995-1004. [doi:10.1016/j.proeng.2010.03.108]

Chen, Q., Kawagoishi, N., Nisitani, H., 2000. Evaluation of fatigue crack growth rate and life prediction of Inconel 718 at room and elevated temperatures. *Materials Science and Engineering: A*, **277**(1-2):250-257.

Chen, Q., Kawagoishi, N., Wang, Q.Y., Yan, N., Ono, T., Hashiguchi, G., 2005. Small crack behavior and fracture of nickel-based superalloy under ultrasonic fatigue. *International Journal of Fatigue*, **27**(10-12):1227-1232. [doi:10.1016/j.ijfatigue.2005.07.022]

Chu, Z.K., Yu, J.J., Sun, X.F., Guan, H.R., Hu, Z.Q., 2008. High temperature low cycle fatigue behavior of a directionally solidified Ni-base superalloy DZ951. *Materials Science and Engineering: A*, **488**(1-2):389-397. [doi:10.1016/j.msea.2007.11.045]

Fedelich, B., 1998. A stochastic theory for the problem of multiple surface crack coalescence. *International Journal of Fracture*, **91**:23-45. [doi:10.1023/A:1007431802050]

Forsyth, P.J.E., 1957. Slip-band damage and extrusion. *Proceedings of the Royal Society of London. Series A, Mathematical and Physical Sciences*, **242**(1229):198-202. [doi:10.1098/rspa.1957.0168]

Fournier, B., Sauzay, M., Caes, C., Noblecourt, M., Mottot, M., Bougault, A., Rabeau, V., Man, J., Gillia, O., Lemoine, P., Pineau, A., 2008. Creep-fatigue-oxidation interactions in a 9Cr-1Mo martensitic steel. Part III: Lifetime prediction. *International Journal of Fatigue*, **30**(10-11):1797-1812. [doi:10.1016/j.ijfatigue.2008.02.006]

Fournier, D., Pineau, A., 1977. Low cycle fatigue behavior of Inconel 718 at 298 K and 823 K. *Metallurgical and Materials Transactions A*, **8**(7):1095-1105. [doi:10.1007/BF02667395]

He, Y.H., Yu, H.C., Guo, W.B., Shen, L.L., Su, B., 2006. Experimental study on fatigue crack growth behavior of direct aging GH4169 superalloy. *Journal of Aerospace Power*, **21**(2):349-353 (in Chinese).

Kobayashi, K., Yamaguchi, K., Hayakawa, M., Kimura, M., 2005. Grain size effect on high-temperature fatigue properties of alloy718. *Materials Letters*, **59**(2-3):383-386. [doi:10.1016/j.matlet.2004.09.029]

Leo Prakash, D.G.L., Walsh, M.J., Maclachlan, D., Korsunsky, A.M., 2009. Crack growth micro-mechanisms in the IN718 alloy under the combined influence of fatigue, creep and oxidation. *International Journal of Fatigue*, **31**(11-12):1966-1977. [doi:10.1016/j.ijfatigue.2009.01.023]

Ma, X.F., Shi, H.J., Gu, J.L., Wang, Z.X., Harders, H., Malow, T., 2008. Temperature effect on low-cycle fatigue behaviour of nickel-based single crystalline superalloy. *Acta Mechanica Solida Sinica*, **21**(4):289-297.

Masuda, C., Tanaka, Y., 1986. Relationship between fatigue strength and hardness for high strength steels. *Transaction of the Japan Society Mechnical Engineers-Part A*, **52**:847-852.

Mercer, C., Soboyejo, A.B.O., Soboyejo, W.O., 1999. Micromechanisms of fatigue crack growth in a forged Inconel 718 nickel-based superalloy. *Materials Science and Engineering: A*, **270**(2):308-322.

Murakami, Y., Kawakami, K., Duckworth, W.E., 1991. Quantitative-evaluation of effects of shape and size of artificially introduced alumina particles on the fatigue-strength of 1.5Ni-Cr-Mo (En24) steel. *International Journal of Fatigue*, **13**(6):489-499.

Pineau, A., 1989. Mechanisms of Creep-fatigue Interactions, Advances in Fatigue Science and Technology. Kluwer Academic, Dordrecht.

Reger, M., Remy, L., 1988a. High-temperature, low-cycle fatigue of IN-100 superalloy. 1. Influence of frequency and environment at high-temperatures. *Materials Science and Engineering: A*, **101**:55-63.

Reger, M., Remy, L., 1988b. High-temperature, low-cycle fatigue of IN-100 superalloy. 1. Influence of temperature on the low-cycle fatigue behavior. *Materials Science and Engineering: A*, **101**:47-54. [doi:10.1016/0921-5093(88)90049-4]

Remy, L., Alam, A., Haddar, N., Köster, A., Marchal, N., 2007. Growth of small cracks and prediction of lifetime in high-temperature alloys. *Materials Science and Engineering: A*, **468-470**:40-50. [doi:10.1016/j.msea.2006.08.133]

Sakai, T., Sato, Y., Oguma, N., 2002. Characteristic S-N properties of high-carbon-chromium-bearing steel under axial loading in long-life fatigue. *Fatigue & Fracture of Engineering Materials & Structures*, **25**(8-9):765-773. [doi:10.1046/j.1460-2695.2002.00574.x]

Sakai, T., Sakai, T., Okada, K., Furuichi, M., Nishikawa, I., Sugeta, A., 2006. Statistical fatigue properties of SCM435 steel in ultra-long-life regime based on JSMS database on fatigue strength of metallic materials. *International Journal of Fatigue*, **28**(11):1486-1492. [doi:10.1016/j.ijfatigue.2005.09.018]

Shiozawa, K., Lu, L., Ishihara, S., 2001. S-N curve characteristics and subsurface crack initiation behaviour in ultra-long life fatigue of a high carbon-chromium bearing steel. *Fatigue & Fracture of Engineering Materials & Structures*, **24**(12):781-790.

Socie, D.F., 1983. Critical Plane Approaches for Multiaxial Fatigue Damage Assessment. ASTM, Philadelphia.

Suresh, S., 1998. Fatigue of Materials. Cambridge University Press, Cambridge, UK.

Tanaka, K., Mura, T., 1981. A dislocation model for fatigue crack initiation. *Journal of Applied Mechanics-Transactions of the ASME*, **48**(1):97-103. [doi:10.1115/1.3157599]

Tomkins, B., 1968. Fatigue crack propagation: an analysis. *Philosophical Magazine*, **18**:1041-1066.

Venkataraman, G., Chung, Y.W., Mura, T., 1991. Application of minimum energy formalism in a multiple slip band model for fatigue—II. Crack nucleation and derivation of a generalised Coffin-Manson law. *Acta Metallurgica et Materialia*, **39**(11):2631-2638. [doi:10.1016/0956-7151(91)90079-G]

Wang, Q.Y., Bathias, C., Kawagoishi, N., Chen, Q., 2002. Effect of inclusion on subsurface crack initiation and gigacycle fatigue strength. *International Journal of Fatigue*, **24**(12):1269-1274. [doi:10.1016/S0142-1123(02)00037-3]

Wang, Q.Y., Kawagoishi, N., Chen, Q., 2006. Fatigue and fracture behaviour of structural Al-alloys up to very long life regimes. *International Journal of Fatigue*, **28**(11):1572-1576. [doi:10.1016/j.ijfatigue.2005.09.017]

Yan, N., Kawagoishi, N., Chen, Q., Wang, Q.Y., Nishitani, H., Kondo, E., 2003. Fatigue properties of Inconel 718 in long life region at elevated temperature. *Key Engineering Materials*, **243-244**:321-326. [doi:10.4028/www.scientific.net/KEM.243-244.321]